IOP Publishing Journal of Optics
J. Opt. 19 (2017) 065804 (8pp) https://doi.org/10.1088/2040-8986/aa7006

Extracting loss from asymmetric resonances in micro-ring resonators

O Reshef, M G Moebius and E Mazur[1]

John A. Paulson School of Engineering and Applied Sciences, Harvard University, 9 Oxford Street, Cambridge, MA 02138, United States of America

E-mail: mazur@seas.harvard.edu

Received 29 January 2017, revised 15 April 2017
Accepted for publication 28 April 2017
Published 19 May 2017

Abstract

Propagation losses in micro-ring resonator waveguides can be determined from the shape of individual resonances in their transmission spectrum. The losses are typically extracted by fitting these resonances to an idealized model that is derived using scattering theory. Reflections caused by waveguide boundaries or stitching errors, however, cause the resonances to become asymmetric, resulting in poor fits and unreliable propagation loss coefficients. We derive a model that takes reflections into account and, by performing full-wave simulations, we show that this model accurately describes the asymmetric resonances that result from purely linear effects, yielding accurate propagation loss coefficients.

Keywords: ring resonators, integrated optics, silicon photonics, propagation losses

(Some figures may appear in colour only in the online journal)

1. Introduction

Ring resonators are one of the simplest and most commonly used components in photonic integrated circuits. Their high quality factors and ease of fabrication in any photonic platform make them useful for applications in wavelength-selective filters and multiplexers [1, 2], optical delay lines [3], switches and modulators [4, 5], and in other nonlinear applications enabled by the resonantly enhanced intensity build-up [6–11]. Additionally, due to their simple analytic transfer function, ring resonators are also used for fabrication characterization; the individual resonances in the transmission spectrum of a ring can be measured and fit to extract propagation losses [12, 13].

This fitting method has been shown to yield accurate propagation losses for ideal devices [12]. However, experimental concerns in real devices often cause resonances to exhibit distortions. This in turn makes it so the transfer function fails to capture all of the physics of the system, thus yielding poor fits. Doing so generates unreliable values for propagation losses, making it more difficult to assess fabrication quality.

There are many reasons why the transfer function of micro-ring resonators might exhibit asymmetries, the most common type of distortion that can reduce the reliability of the fitting process. For example, nonlinear interactions, such as by optical bistability, are known to cause asymmetries [14–16]. In terms of linear devices, roughness-induced coherent back-scattering or polarization rotation within the ring has been shown to generate significant frequency domain distortions as well as resonance-splitting [17–23]. Another possible source for asymmetric resonances are fabrication imperfections in the directional coupler of the ring [24].

Aside from these considerations that originate within the ring itself, back-reflections from *outside* of the ring, which are common in realistic devices, can also yield asymmetries in the resonances that are linear in origin [25–30]. For example, polarization mixing or fabrication defects in the waveguide leading to and from the resonator can cause partial reflections that yield asymmetric Fano-like resonances in the otherwise symmetric spectrum of a ring resonator [5, 18, 25, 26, 29]. These asymmetries are most prevalent in smaller, low-loss systems with high quality factors, and pose an increasing challenge as fabrication quality further improves.

A significant amount of work has already been done on coupled-cavity formalisms, even in the context of integrated circuits [19, 23, 27, 31, 32]. Here, we treat the specific case for extracting propagation losses from a micro-ring resonator. We generalize the familiar transfer function for micro-ring resonators to develop a model that includes the interference caused by

[1] Author to whom any correspondence should be addressed.

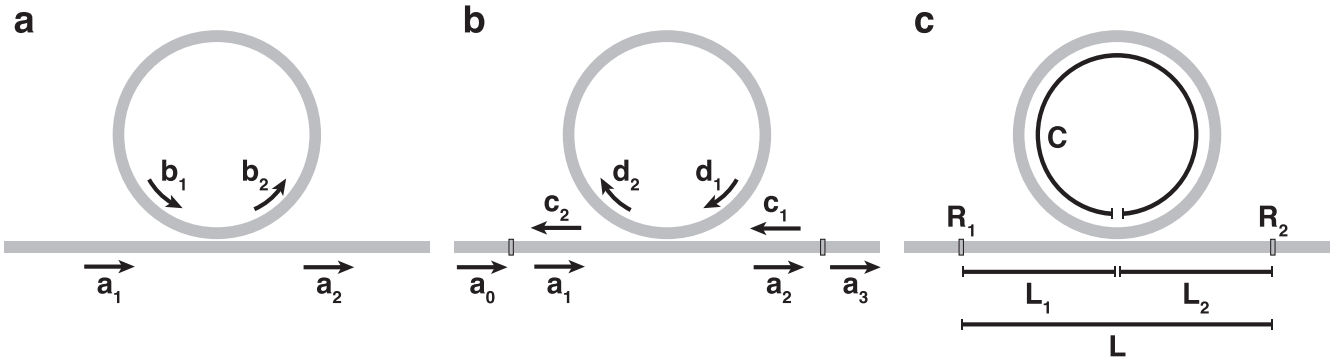

Figure 1. (a) The right-traveling field in the waveguide excites a counter-clockwise-propagating mode b_2 and another right-traveling mode a_2. These two modes interfere destructively when operating on resonance. (b) Partial reflectors at the input and output of the waveguide enable left-traveling fields and clockwise-propagating modes. These fields form a secondary resonance (i.e., $a_1 \rightarrow a_2 \rightarrow c_1 \rightarrow c_2 \rightarrow a_1$) that interferes with the whispering gallery modes in the ring to produce asymmetries in the combined spectrum. (c) The simulated device: a ring resonator of circumference C coupled to a bus waveguide of length L between a pair of reflectors R_1 and R_2.

accidental reflections in waveguides. Using full-wave simulations we demonstrate that these asymmetries are caused by reflections and are independent of input power. We also discuss situations in which reflections become significant. We use this generalized transfer function to extract the propagation loss of the simulated devices, and demonstrate that the model remains reliable in the presence of strong reflections, unlike the standard symmetric model. This generalized transfer function is important in the experimental characterization of micro-ring resonators with inherent reflections.

2. Theory

2.1. Standard symmetric transfer function

The transmission of a micro-ring resonator coupled to a single waveguide (i.e., an input port and no add or through port) has been well characterized and can be derived using scattering theory [12, 16, 33–35]. We begin by describing the set of interactions that yield the standard symmetric transfer function. The complete set of electric fields is illustrated in figure 1. The input and output fields are denoted by a_1 and a_2, respectively. The input field a_1 is incident on a directional coupler which excites a counter-clockwise-propagating mode b_2:

$$b_2 = \sqrt{1 - t^2}\, a_1, \tag{1}$$

where t is the transmission (or self-coupling) coefficient that corresponds to the field that remains in the waveguide after traversing the coupling region.

While propagating through the circumference C of the ring, the field b_2 accumulates a phase $\phi = \omega C/c = 2\pi n_{\text{eff}} C/\lambda$ and experiences a propagation loss α_z due to scattering and fabrication imperfections, yielding a field b_1:

$$b_1 = \mathrm{e}^{-\alpha_z C/2}\mathrm{e}^{\mathrm{i}\phi} b_2. \tag{2}$$

The total propagation loss in the ring is denoted by α:

$$\alpha^2 \equiv \mathrm{e}^{-\alpha_z C}, \tag{3}$$

so that $\alpha \rightarrow 1$ in the lossless case and $\alpha \rightarrow 0$ as the propagation loss approaches infinity. The loss coefficient α represents all of the loss mechanisms in the system, including contributions from waveguide scattering, bending losses and the excess insertion losses of the directional coupler.

Part of the field b_1 couples back into b_2. Adding this contribution to equation (1), we obtain:

$$b_2 = \sqrt{1 - t^2}\, a_1 + t b_1 = \sqrt{1 - t^2}\, a_1 + t\alpha \mathrm{e}^{\mathrm{i}\phi} b_2. \tag{4}$$

The total output field a_2 is the sum of the field that is directly transmitted from a_1 through the coupler and the field that couples back from the ring from b_1:

$$a_2 = t a_1 - \sqrt{1 - t^2}\, b_1 = t a_1 - \sqrt{1 - t^2}\, \alpha \mathrm{e}^{\mathrm{i}\phi} b_2. \tag{5}$$

The transmission for the ring resonator $T_{\text{RR}}(\phi)$ is the solution of the coupled equations (4) and (5):

$$\begin{aligned} T_{\text{RR}}(\phi) &\equiv \left| \frac{a_2}{a_1} \right|^2 = \left| \frac{t - \alpha \mathrm{e}^{\mathrm{i}\phi}}{1 - \alpha t \mathrm{e}^{\mathrm{i}\phi}} \right|^2 \\ &= \frac{t^2 + \alpha^2 - 2\alpha t \cos\phi}{1 + \alpha^2 t^2 - 2\alpha t \cos\phi}. \end{aligned} \tag{6}$$

Both parameters α and t are dimensionless and range from 0 to 1. $T_{\text{RR}}(\phi)$ is a symmetric function of ϕ, which only appears in the argument of a cosine. The transfer function also remains symmetric upon interchanging α and t, as is seen more evidently in the expanded equation (6). As a consequence, the two coefficients contribute similarly to the transfer function and thus are often difficult to distinguish when fitting [12, 36]. They can be disentangled by fitting to resonances measured from multiple devices or to a range of resonances from a single device because the propagation loss is expected to remain constant as a function of wavelength or other device parameters (e.g., coupling gap, ring radius), whereas the coupling coefficient should vary [12, 37].

2.2. Asymmetric transfer function

We now add a pair of partial reflectors with reflectivities R_1 and R_2 to the waveguide in locations that surround the ring at distances L_1 and L_2 away, respectively (figure 1(c)). The additional fields that are introduced are illustrated in figure 1(b).

The original output a_2 now excites an output a_3 that is behind a partial reflector R_2:

$$a_3 = \sqrt{1 - R_2^2}\, e^{-\alpha_z L_2/2} e^{i\varphi_2} a_2. \tag{7}$$

With the reflector in place, the mode a_2 now also excites a left-traveling wave c_1, yielding the following relation:

$$e^{-\alpha_z L_2/2} e^{i\varphi_2} c_1 = R_2 e^{-\alpha_z L_2/2} e^{i\varphi_2} a_2. \tag{8}$$

Both terms include the accumulated loss and an additional phase term φ_2 accumulated while propagating over the length L_2.

The left-traveling wave c_1 excites a clockwise-propagating wave d_2. The field d_2 propagates through the circumference of the ring and excites another left-traveling wave c_2. The interaction is described by a pair of equations that are analogous to equations (4) and (5):

$$d_2 = \sqrt{1 - t^2}\, c_1 + t\alpha e^{i\phi} d_2, \tag{9}$$

$$c_2 = t c_1 - \sqrt{1 - t^2}\, \alpha e^{i\phi} d_2. \tag{10}$$

The left-traveling wave c_2 reflects from the partial reflector R_1 and contributes to input a_1, yielding:

$$a_1 = \sqrt{1 - R_1^2}\, e^{-\alpha_z L_1/2} e^{i\varphi_1} a_0 - R_1 e^{-\alpha_z L_1/2} e^{i\varphi_1} c_2, \tag{11}$$

where φ_1 corresponds to the phase accumulated over the length L_1.

Equations (7)–(11), along with equations (4) and (5), constitute the complete set of coupled equations. Solving for the transmission yields our final equation:

$$T(\phi) = \left| \frac{a_3}{a_0} \right|^2 = (1 - R_1^2)(1 - R_2^2) e^{-\alpha_z L} \times \left| \frac{(1 - \alpha t e^{i\phi})(t - \alpha e^{i\phi})}{(\alpha t e^{i\phi} - 1)^2 - \gamma e^{i\varphi}(\alpha e^{i\phi} - t)^2} \right|^2, \tag{12}$$

with the substitutions:

$$\gamma \equiv |R_1 R_2 e^{-\alpha_z L}| \tag{13}$$

$$\varphi \equiv 2\pi (2L) n_{\text{eff}} / \lambda + \varphi_0. \tag{14}$$

The additional coefficients γ and φ correspond to the loss and phase contributed by the bus waveguide, respectively. This result includes a new term, $e^{-\alpha_z L}$, accounting for the propagation loss through the waveguide between the partial reflectors, and a new pair of phase terms: $2\pi (2L) n_{\text{eff}} / \lambda$, which accumulates along the length of the waveguide, and a phase offset φ_0, which is introduced by the reflections. Equations (13) and (14) reveal that the strength and shape of the asymmetry only depend on the total round trip length $2L$, and not on the respective distance to the reflectors L_1 and L_2.

As expected, this result reduces to the ideal case (equation (6)) when the mirrors are removed (R_1, $R_2 \to 0$). If we have no coupling to the ring ($t \to 1$), we obtain the transmission for a Fabry–Perot etalon of length L with a pair of boundaries with reflectivity R_1 and R_2 [35],

$$T_{\text{Fabry–Perot}}(\varphi) = \left| \frac{\sqrt{1 - R_1^2}\sqrt{1 - R_2^2}\, e^{-\alpha_z L/2}}{1 - R_1 R_2 e^{i\varphi} e^{-\alpha_z L}} \right|^2. \tag{15}$$

We scale equation (12) so that the peak value measured at the output is 1. Doing so normalizes away any variables that are not explicit functions of ϕ or φ, and yields:

$$\tilde{T}(\phi) = \left| \frac{(1 - \alpha t e^{i\phi})(t - \alpha e^{i\phi})}{\gamma e^{i\varphi}(t - \alpha e^{i\phi})^2 - (1 - \alpha t e^{i\phi})^2} \right|^2 = T_{\text{RR}}(\phi) \left| \frac{1}{1 - \gamma e^{i\varphi} T_{\text{RR}}(\phi)} \right|^2. \tag{16}$$

Equation (16) shows that $\tilde{T}(\phi)$ is just $T_{\text{RR}}(\phi)$ with a correction term tuned by the asymmetry parameter γ.

We will show that this equation can be used to extract propagation losses, even in the presence of strong boundary reflections.

2.3. Asymmetry threshold

If the reflections R_1 or R_2 are small and the bus waveguide is very long, the asymmetry parameter γ is correspondingly small. One might expect the asymmetric correction to $T_{\text{RR}}(\phi)$ to become negligible. However, even small γ values can lead to pronounced asymmetries in some configurations. The term with γ in the denominator dominates when

$$1 \ll \left| \frac{2\gamma e^{i\varphi}(t - \alpha e^{i\phi})^2}{(1 - \alpha t e^{i\phi})^2} \right|. \tag{17}$$

This means that the reflection term γ needs to be larger than a threshold value of

$$\gamma_{\text{threshold}} \equiv \frac{(1 - \alpha t)^2}{2|t + \alpha|^2}. \tag{18}$$

We expect reflections (and thus γ) to be very small so as not to observe any asymmetries. However, equation (18) shows that it is easy to obtain asymmetric resonances if both α and t approach 1, as is generally desired. As was mentioned previously, large values of α correspond to smaller rings or low propagation losses.

For example, for a ring resonator with a diameter of 100 μm and a propagation loss of 0.1 dB mm^{-1}, $\alpha \approx 0.99$ (neglecting the insertion loss of the directional coupler). In this case, $\gamma_{\text{threshold}} \approx 10^{-5}$, and so just 0.25% (−26 dB) reflections at the boundaries are necessary to cause noticeable asymmetries. A reflection this low is easily produced as a byproduct of a *Y*-junction splitter or a multimode interferometer, among other commonly used integrated photonic components. Above this threshold, the standard symmetric transfer function begins to fail. Functionally, this means that asymmetries can be suppressed in systems with considerable propagation loss or with large rings. This low threshold also explains why asymmetries are so common in high-Q systems, and why it is hard to estimate the propagation loss using rings in low-loss systems.

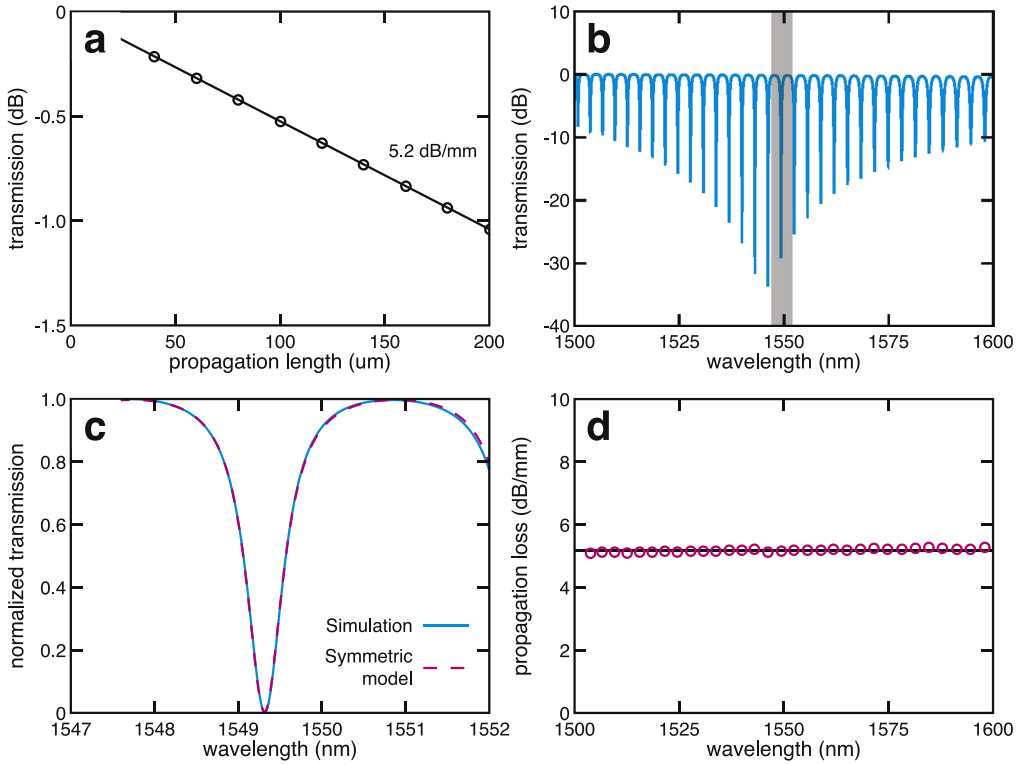

Figure 2. (a) We obtain a propagation loss of 5.2 dB mm^{-1} for the waveguide used in the resonator by fitting to the transmission of a straight waveguide and extracting the slope. (b) The transmission spectrum for TM-polarized light in a micro-racetrack resonator with a total circumference of 400 μm. We observe near-critical coupling throughout the wavelength range, peaking around $\lambda = 1550$ nm. (c) We fit to the resonance in the shaded region in (b) and obtain $\alpha = 0.774$. (d) Extracted propagation loss from each individual resonance in (b) (circles). The mean propagation loss is 5.2 dB mm^{-1}, in agreement with the value fit in (a).

3. Results and discussion

3.1. Device geometry and simulation parameters

We use a commercial two-dimensional finite difference time domain (2D-FDTD) solver and the effective index method [38] to simulate a micro-ring resonator in order to verify these equations. The device we model consists of a lossy silicon ($n = 3.5 + 0.0002i$) micro-racetrack resonator on a silica ($n = 1.45$) substrate. The racetrack is formed of waveguides that are etched from a 220 nm thick silicon slab and have a horizontal width of 300 nm. We set the constituent materials to be dispersionless to simplify the model and to prove that these asymmetric artifacts are independent of any specific material dispersion. The resonator parameters include a coupling length of 10 μm, an edge-to-edge coupling gap of 90 nm and a total ring circumference of 400 μm. This device is designed to achieve critical-coupling for TM-polarized light in the center of the telecom operation range, at $\lambda = 1550$ nm. The imaginary component of the index is selected to achieve a propagation loss near 5 dB mm^{-1} (figure 2(a)). Though this loss might appear significant, we use a small ring for α to remain large enough ($\alpha \approx 0.75$) so as not to suppress the effects we are studying. Both of these factors contribute to minimizing the simulation time. The complete set of parameters is summarized in table 1.

Table 1. Device geometry.

Material index	$3.5 + 2 \times 10^{-4}i$
Substrate index	1.45
Waveguide width	300 nm
Waveguide height	220 nm
Ring circumference	400 μm
Coupling length	10 μm
Gap size	90 nm

The effective index method yields an effective index of $n_{\text{eff}} = 1.93$ for the waveguide and $n_{\text{eff}} = 1$ for all other regions. We calculate the propagation loss for TM-polarized light at $\lambda = 1550$ nm by performing a virtual cut-back method [39]; we monitor the transmitted light at various positions in the waveguide and perform a linear fit (figure 2(a)), yielding a propagation loss of 5.2 dB mm^{-1}. For the given ring circumference and propagation loss we calculate the loss coefficient at $\lambda = 1550$ nm to be $\alpha = 0.775$. The predicted α also includes the minimal scattering loss that results from the mode mismatch between the straight and bent parts of the racetrack resonator (0.2% per junction), but neglects the insertion loss of the directional coupler. Given the selected parameters, we estimate the maximum loaded Q-factor to be $Q = \pi n_g/(\alpha_z \lambda) = 3.3 \times 10^3$ [40].

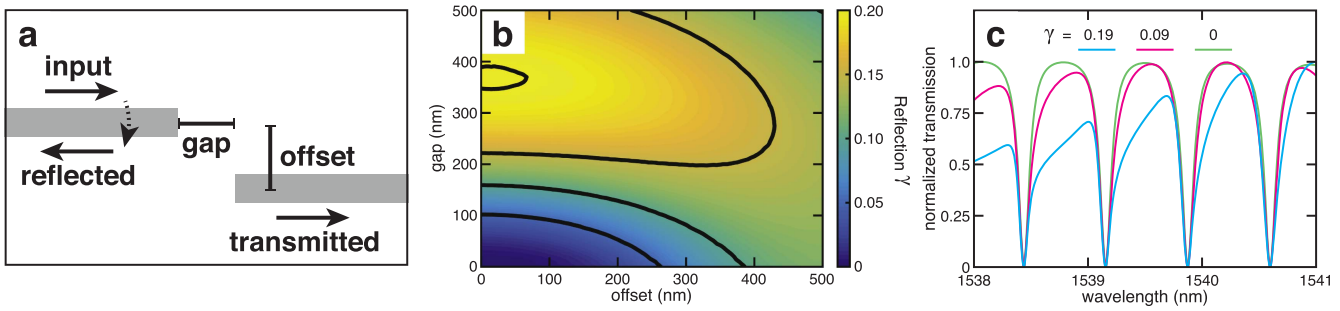

Figure 3. (a) Top-down view of a pair of stitching errors in the waveguide surrounding the ring resonator. They can behave as the partial reflectors in figure 1(b) and cause asymmetries to form in the transmission spectrum of a ring resonator. We describe these errors using two parameters, an offset and a gap. (b) Retrieved γ (corresponding to $|R_1 R_2|$) for different offsets and gaps. (c) As the reflections included in the simulation become important, the asymmetries become more pronounced without displacing the original resonances.

3.2. Symmetric resonances

Before tackling the asymmetric case with paired partial reflections, we begin by simulating an ideal ring resonator to demonstrate the propagation loss extraction method [12]. The transmission for TM-excitation in the geometry described above is shown in figure 2(b). We observe equally spaced symmetric resonance peaks with an average free spectral range of 3.14 nm (390 GHz). They possess extinction ratios in excess of 10 dB throughout the range of operation, confirming that the resonator is near-critically coupled to the waveguide. The largest extinction ratio observed (33 dB) is located at $\lambda = 1546.2$ nm, at the center of the operation range. This resonance has a loaded Q-factor of 3.0×10^3. The resonances ranging from $\lambda = 1500$ to 1600 nm are fit to the traditional transfer function in equation (6), allowing the transmission coefficient t and the total loss coefficient α to vary independently. A representative fit is shown in figure 2(c). The fits are consistently well-behaved, and yield a loss parameter α for each resonance. We calculate the propagation losses α_z for each resonance using equation (3) and plot them in figure 2(d). The loss values extracted using this method consistently agree well with the propagation loss in figure 2(a), with a geometric mean of 5.2 dB mm^{-1}. This result demonstrates that fitting to equation (6) is a reliable method for estimating the propagation loss of a waveguide for symmetric resonances.

3.3. Asymmetric resonances

In order for asymmetries to appear in the simulated transmission spectrum, partial reflectors must be placed into the waveguide. We choose to insert artificial stitching errors to act as reflectors, as they are simple to model and fully characterize using FDTD. These errors routinely appear during the electron-beam lithography process and are caused by the drift of successive write-windows, manifesting as horizontal displacements in the plane of the device layer (figure 3(a)). We simulate the reflection coefficient for different gaps and offsets that might result from a stitching error (figure 3(b)). For a perfectly aligned pair of waveguides (i.e., no stitching error) none of the light is reflected back towards the input, as expected. As the gap or offset increases, the reflected field grows. Counter-intuitively, above a certain gap size the reflected field decreases. This decrease is due to interference effects from the combined field within the gap—the field reflected from the end of the input waveguide interferes destructively with the field reflected from the beginning of the second waveguide. Figure 3(b) shows that stitching errors in our system yield a maximum reflection value of $\gamma = 0.2$. With $\alpha = 0.775$, equation (18) predicts that we need $\gamma > \gamma_{\text{threshold}} = 0.029$ before the transmission spectrum from the simulated device exhibits significant asymmetries.

We set the partial reflectors in our device to be stitching gaps that are 17 μm apart, surrounding the ring-coupling region. This length was chosen because it is not a multiple of the ring circumference (400 μm). If the spacing between the reflectors is much larger than the circumference of the ring, a ripple will form in the transfer function instead of an asymmetry. The elimination of this type of artifact has already been treated elsewhere in the literature [31]. We compare the effect of different asymmetry parameters γ by simulating devices with different stitching gap sizes of 300 nm (corresponding to $\gamma = 0.1902$), 200 nm ($\gamma = 0.1339$), 150 nm ($\gamma = 0.0921$), 100 nm ($\gamma = 0.0484$), 70 nm ($\gamma = 0.0259$) and 35 nm ($\gamma = 0.0053$). In figure 3(c), we plot the transmission for the most extreme case with a gap size of 300 nm and the median case, with a gap size of 150 nm. We compare them to the ideal case from the previous section. As expected, the asymmetry increases with increasing γ. We have purposely chosen to implement unphysically large reflections in our simulation in order to compensate for the large propagation loss that was necessary for the convergence of the simulation. However, though undesired reflections in realistic integrated photonics circuits are likely to be smaller in physical implementations, pronounced asymmetries will still manifest so long as the propagation losses are low enough to satisfy the the asymmetry criteria outlined in section 2.3.

The complete transmission spectrum for the device with the largest gap is shown in figure 4(a). The familiar resonance peaks from figure 2(b) are superimposed with a slower secondary oscillation which adds characteristic asymmetries to the individual resonances. The resonances now also appear to possess different extinction ratios than their idealized counterparts. However, this apparent difference is an artifact of the superposition between the two oscillations.

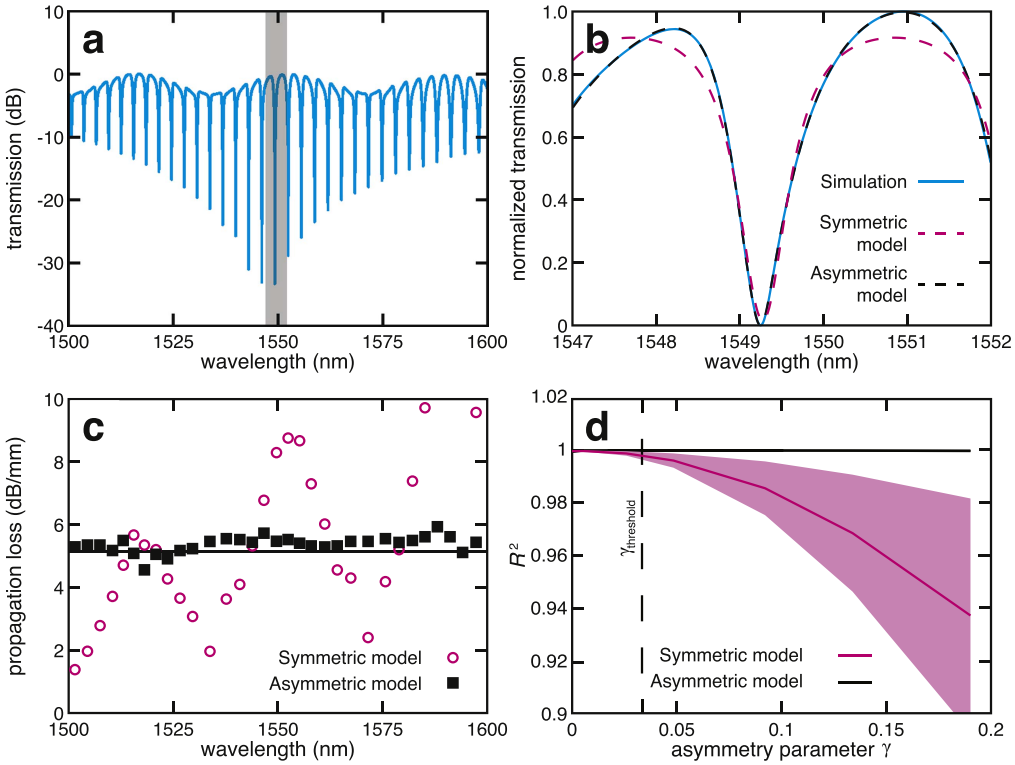

Figure 4. (a) Transmission over the entire operation range for the device described in section 3.3. (b) Fits to the resonance in the shaded area in (a), using both the standard symmetric model (red) and the asymmetric model developed in this work (black). The symmetric model fits the center of the resonances but is incapable of capturing the complete physics of the resonance. (c) The asymmetric model predicts a propagation loss of 5.4 dB mm^{-1} while the symmetric model predicts an average propagation loss of 5.0 dB mm^{-1}. However, the standard symmetric model exhibits much larger oscillating deviations. (d) Shaded error bar plot of averaged R^2 values of the fit to the transmission spectrum as a function of asymmetry γ. The R^2 values remain constant for all fits to the asymmetric model proposed in this work. On the other hand, the fit quality for the standard model declines once $\gamma > \gamma_{\text{threshold}}$.

We fit these resonances using both the standard symmetric transfer function $T_{RR}(\phi)$, and the asymmetric transfer function $\tilde{T}(\phi)$ (figure 4(b)). In simulation we know the length of the bus waveguide between the reflectors; however, if this length is unknown, its value could easily be determined by taking the Fourier transform of the measured transmission. The propagation loss extracted using both the symmetric and asymmetric transfer functions are plotted in figure 4(c). The asymmetric function consistently predicts an average propagation loss of 5.4 dB mm^{-1} with a geometric standard deviation of 1.05, in agreement with the value extracted from the cut-back simulation and the symmetric fits in figure 2. On the other hand, the standard transfer function $T_{RR}(\phi)$ predicts an average loss of 5.0 dB mm^{-1} with a geometric standard deviation of 1.70. This large standard deviation is evident in the dramatic oscillations about the mean, with values ranging from 1.4 to 11.6 dB mm^{-1}. The asymmetric function fits the data significantly better when strong reflections are present. To demonstrate this quantitatively, we calculated the average R^2 for the fits in each spectrum. As can be seen in figure 4(d), both transfer functions fit the data well when $\gamma < \gamma_{\text{threshold}} = 0.029$, but above this value the standard symmetric transfer function deviates significantly from $R^2 = 1$ with a large range of R^2 values, whereas the asymmetric transfer function remains at $R^2 = 1$ for every resonance.

4. Conclusion

We demonstrated that asymmetric resonances can result from purely linear effects in micro-ring resonators, such as partial reflections that are unavoidable in a realistic device or experimental setup. We derived and numerically verified a threshold above which the asymmetries become pronounced. Realistic devices easily exceed this threshold and therefore exhibit asymmetric resonances. The asymmetries are most pronounced in low-loss systems, where they appear for boundary reflections on the order of 1% or less. The reflectors do not need to be as close to each other as they are in this work—the asymmetries described in this work can just as easily originate from waveguide boundaries when the total waveguide length is comparable to the resonator length.

We derived a new transfer function that takes these asymmetries into account. The equations in this model reduce to their symmetric counterparts in the special case of negligible reflections. This asymmetric transfer function outperforms the standard symmetric transfer function at modeling resonances from a ring resonator when the reflections are significantly above the threshold. The standard ring transfer function is therefore unreliable at extracting propagation losses, and the new asymmetric transfer function derived in this paper should be used in its place. As material deposition

and fabrication techniques improve, losses will decrease and *Q*-factors will increase, exacerbating the prevalence of asymmetries in state-of-the-art devices and thus the need for a new model that can account for asymmetries.

Acknowledgments

Several people contributed to the work described in this paper. OR conceived of the basic idea for this work, performed the simulations and analyzed the results. MGM helped perform the derivations and analysis. EM supervised the research and the development of the manuscript. The authors declare no competing financial interests. The authors acknowledge the help of Daryl I Vulis and Philip Camayd-Muñoz with FDTD and the help of Kelly Anne Miller with statistical analysis. OR wrote the first draft of the manuscript; all authors subsequently took part in the revision process and approved the final copy of the manuscript. Olivia Mello, Kelly Anne Miller and Dario Rosenstock provided feedback on the manuscript throughout its development. The authors thank Katia Shtyrkova, Jeremy Upham and Sebastian A Schulz for helpful discusisons. The research described in this paper was supported by the National Science Foundation under contracts ECCS-1201976 and PHY-1415236. OR acknowledges support from the Natural Sciences and Engineering Research Council of Canada.

References

[1] Little B E, Chu S T, Haus H A, Foresi J and Laine J P 1997 Microring resonator channel dropping filters *J. Lightwave Technol.* **15** 998–1005
[2] Barwicz T *et al* 2004 Microring-resonator-based add-drop filters in SiN: fabrication and analysis *Opt. Express* **12** 1437–42
[3] Boyd R W, Gauthier D J and Gaeta A L 2006 Applications of slow light in telecommunications *Opt. Photonic News* **17** 18–23
[4] Almeida V R, Barrios C A, Panepucci R R and Lipson M 2004 All-optical control of light on a silicon chip *Nature* **431** 1081–4
[5] Dong P, Preble S F and Lipson M 2007 All-optical compact silicon comb switch *Opt. Express* **15** 9600–5
[6] Heebner J E, Boyd R W and Park Q-H 2002 Slow light, induced dispersion, enhanced nonlinearity, and optical solitons in a resonator-array waveguide *Phys. Rev.* E **65** 036619
[7] Foster M A *et al* 2006 Broad-band optical parametric gain on a silicon photonic chip. *Nature* **441** 960–3
[8] Levy J S *et al* 2010 CMOS-compatible multiple-wavelength oscillator for on-chip optical interconnects *Nat. Photon.* **4** 37–40
[9] Kippenberg T J, Holzwarth R and Diddams S A 2011 Microresonator-based optical frequency combs *Science* **332** 555–9
[10] Okawachi Y *et al* 2011 Octave-spanning frequency comb generation in a silicon nitride chip *Opt. Lett.* **36** 3398–400
[11] Hausmann B J M, Bulu I, Venkataraman V, Deotare P and Lončar M 2014 Diamond nonlinear photonics *Nat. Photon.* **8** 369–74
[12] McKinnon W R *et al* 2009 Extracting coupling and loss coefficients from a ring resonator *Opt. Express* **17** 18971–82
[13] Reshef O *et al* 2015 Polycrystalline anatase titanium dioxide microring resonators with negative thermo-optic coefficient *J. Opt. Soc. Am.* B **32** 2288–93
[14] Heebner J E and Boyd R W 1999 Enhanced all-optical switching by use of a nonlinear fiber ring resonator *Opt. Lett.* **24** 847–9
[15] Almeida V R and Lipson M 2004 Optical bistability on a silicon chip *Opt. Lett.* **29** 2387–9
[16] Bogaerts W *et al* 2012 Silicon microring resonators *Laser Photonics Rev.* **6** 47–73
[17] Gorodetsky M *et al* 2000 Rayleigh scattering in high-*Q* microspheres *J. Opt. Soc. Am.* B **17** 1051–7
[18] Morichetti F, Melloni A and Martinelli M 2006 Effects of polarization rotation in optical ring-resonator based devices *J. Lightwave Technol.* **24** 573–85
[19] Zhang Z, Dainese M, Wosinski L and Qiu M 2008 Resonance-splitting and enhanced notch depth in SOI ring resonators with mutual mode coupling *Opt. Express* **16** 4621–30
[20] Morichetti F *et al* 2010 Coherent backscattering in optical microring resonators *Appl. Phys. Lett.* **96** 081112
[21] Ballesteros G C, Matres J, Martí J and Oton C J 2011 Characterizing and modeling backscattering in silicon microring resonators *Opt. Express* **19** 24980–5
[22] Ji X *et al* 2016 Breaking the loss limitation of on-chip high-confinement resonators arXiv:1609.08699
[23] Li A, Van Vaerenbergh T, De Heyn P, Bienstman P and Bogaerts W 2016 Backscattering in silicon microring resonators: a quantitative analysis *Laser Photonics Rev.* **10** 420–31
[24] Cusmai G, Morichetti F, Rosotti P, Costa R and Melloni A 2005 Circuit-oriented modelling of ring-resonators *Opt. Quantum Electron.* **37** 343–58
[25] Fan S 2002 Sharp asymmetric line shapes in side-coupled waveguide-cavity systems *Appl. Phys. Lett.* **80** 908–10
[26] Choy J T *et al* 2012 Integrated TiO_2 resonators for visible photonics *Opt. Lett.* **37** 539–41
[27] Hu T *et al* 2013 Tunable Fano resonances based on two-beam interference in microring resonator *Appl. Phys. Lett.* **102** 011112
[28] Luk'yanchuk B *et al* 2010 The Fano resonance in plasmonic nanostructures and metamaterials *Nat. Mater.* **9** 707–15
[29] Liang W *et al* 2006 Transmission characteristics of a Fabry–Perot etalon-microtoroid resonator coupled system *Opt. Lett.* **31** 510–2
[30] Li B B *et al* 2011 Experimental observation of Fano resonance in a single whispering-gallery microresonator *Appl. Phys. Lett.* **98** 021116
[31] Strain M J, Gnan M, Bellanca G, De La Rue R M and Sorel M 2009 Retrieval of Bragg grating transmission spectra by post-process removal of spurious Fabry–Perot oscillations *Opt. Express* **17** 13493–501
[32] Wu Y-D 2014 New design of triplexer based on metal-insulatormetal plasmonic ring resonators *Chin. Opt. Lett.* **12** 110607
[33] Yariv A 2000 Universal relations for coupling of optical power between microresonators and dielectric waveguides *Electron. Lett.* **36** 321–2
[34] Heebner J E, Wong V, Schweinsberg A, Boyd R W and Jackson D J 2004 Optical transmission characteristics of fiber ring resonators *IEEE J. Quantum Electron.* **40** 726–30
[35] Yariv A 1991 *Optical Electronics* 4th edn (Philadelphia, PA: Saunders)
[36] Rasoloniaina A *et al* 2014 Controling the coupling properties of active ultrahigh-Q WGM microcavities from undercoupling to selective amplification *Sci. Rep.* **4** 4023

[37] Delâge A *et al* 2009 Wavelength-dependent model of a ring resonator sensor excited by a directional coupler *J. Lightwave Technol.* **27** 1172–80

[38] Hammer M and Ivanova O V 2009 Effective index approximations of photonic crystal slabs: a 2-to-1-D assessment *Opt. Quantum Electron.* **41** 267–83

[39] Vlasov Y and McNab S 2004 Losses in single-mode silicon-on-insulator strip waveguides and bends *Opt. Express* **12** 1622–31

[40] Preston K, Schmidt B and Lipson M 2007 Polysilicon photonic resonators for large-scale 3D integration of optical networks *Opt. Express* **15** 17283–90